https://doi.org/10.5194/egusphere-2024-404
Preprint. Discussion started: 22 March 2024

Effects of spatial resolution of digital terrain obtained by drone on mountainous urban fluvial flood modelling

Xingyu Zhou [1, 2], Lunwu Mou [3], Tianqi Ao[1, 2], Xiaorong Huang [1, 2], Haiyan Yang [3,4]

[1] State Key Laboratory of Hydraulics and Mountain River Engineering, Sichuan University, Chengdu 610065, China
[2] College of Water Resource & Hydropower, Sichuan University, Chengdu 610065, China
[3] Sichuan Dazhou Hydrological and Water Resources Survey Centre, Dazhou 635000, China
[4] School of Water Conservancy, North China University of Water Resources and Electric Power, Zhengzhou 450046, China

Correspondence to: Xiaorong Huang (hxiaorong@scu.edu.cn)

Abstract: The effect of resolution and quality of terrain data, as the most sensitive input to 2D hydrodynamic modelling, has been one of the main research areas in flood modelling. However, previous studies have lacked the discussion on the limitation of the target area and the data source, as well as the underlying causes of simulation bias due to different resolutions. This study first discusses the performance of high-resolution DSM acquired by drone for flood modelling in a mountainous riverine city, and the effect of DSM resolution on results using grid resolutions from 6 cm to 30 m. The study then investigates the root causes of the effect based on topographic attributes. Xuanhan city, a riverine city in the mountainous region of southwest China, was used as the study area. The HEC-RAS 2D model was used for all simulations, and the results generated using 6 cm DSM acquired by drone were used as a benchmark. Results show that the simulation effect of flood characteristics shows a certain step change with the change of DSM resolution. DSMs with a resolution within 10 m can better capture the undulating features of the topography in the study area, which is crucial for the modelling of the inundation area. However, if features with specific elevation difference values are involved, it is best to keep the resolution within 5 m, which will have a direct impact on the accuracy of the modelling of the flood depth. The analysis of topographic attributes provides theoretical support for obtaining the optimal resolution to match simulation requirements.

Keywords: Drone, digital surface model, spatial resolution, urban fluvial flood modelling, mountainous topographic attributes

1 Introduction

In the past decade, floods, storms and droughts together have caused 80%-90% of the worldwide natural disasters, with floods accounting for more than 40% (WHO,2020). More than 2 billion people worldwide were affected by flood events,and their death toll accounted for half of all deaths caused by natural disasters (Alderman et al., 2012;Samela et al., 2016). With the continuous development of residential areas on the flood plains and the increase of extreme precipitation events caused by the

El Niño phenomenon induced by global warming, nearly 40% of the global cities will be located in flood-prone areas by 2030, especially the mountainous cities along the rivers (Güneralp et al., 2015; Corringham and Cayan, 2019; Muthusamy et al., 2021).

Taking the southwest mountainous area of China as an example, influenced by the complex topography and steep terrain, a large number of towns have chosen to expand along the major rivers in the past few decades. Different from the urban waterlogging caused by the impermeable surface and drainage network in the plain cities, for the mountainous cities along the rivers, on the one hand, the steep terrain accelerates the process of runoff entering the river during heavy rain, on the other hand, the financial budget and planning foresight were limited in the early urban construction, the construction standards of the river flood control projects were generally low and the residential areas were set up irrationally, resulting in their inundation mainly affected by the rapid rise and fall of the river floods. Facing climate change and extreme weather, flood inundation will bring far more than expected damage (Xing et al., 2018; Utlu and Özdemir, 2021). Therefore, understanding the potential flood inundation areas of the mountainous cities along the rivers is essential for assessing flood risk and future planning. Hydrodynamic flood modelling methods play a crucial role in flood inundation simulation and risk management, and various GIS-based hydrodynamic flood models have been developed in recent years (Azizian and Brocca, 2020; Utlu and Özdemir, 2021).

Using hydrodynamic models for flood risk assessment and management requires various types of data, such as topography and hydrological data. In the past decade, the rapid development of satellite remote sensing technology and computer performance has enabled the wider application of 2D hydrodynamic models for flood modelling (Bates, 2012; Yan et al., 2015; Utlu and Ozdemir, 2020). The most sensitive input affecting the 2D flood inundation simulation attributes (depth, extent, velocity) is the digital elevation model (DEM), which places higher requirements on the quality and resolution of the DEM (Cook and Merwade, 2009; da Costa et al., 2019). Currently, the freely available global DEM data with different resolutions are mainly derived from satellite imagery, such as SRTM DEM (30-90m), ASTER GDEM (30m), MERIT DEM (90m), ALOS DEM (12.5-30m). Coarse resolution DEM (>30m) can meet the simulation needs of large-scale flood events in large basins, but it is difficult to accurately capture the topographic features of mountainous areas or complex urban environments (Saksena and Merwade, 2015; Ogania et al., 2019; Utlu and Özdemir, 2021). Developed countries could use satellite- and airborne-based lidar or synthetic aperture radar to obtain Digital Terrain Models (DTMs) and Digital Surface Models (DSMs) with more topographic details, with resolution accuracy up to centimeter level (Md Ali et al., 2015).

https://doi.org/10.5194/egusphere-2024-404
Preprint. Discussion started: 22 March 2024

In recent years, drone technology has developed rapidly, and civilian small-scale drones, equipped with functionalities such as flight path planning, automatic flight control, and mountable sensors, have successfully overcome the challenges of traditional drone surveying equipment, including inconvenient portability, high operational thresholds, and costs. The civilian drones are now widely applied in various fields such as hydrology, agriculture, and forestry (Castaldi et al., 2017; Loladze et al., 2019; Acharya et al., 2021). Using drones to obtain high-resolution DSMs is not easily constrained by time and space, and could be deployed on demand. This provides a reliable terrain input for precise and accurate inundation simulation of 2D hydraulic models (Meesuk et al., 2015; Cook, 2017). Theoretically, as long as the model can process high-resolution DSM, the higher the resolution, the more accurate the simulation results produced (Muthusamy et al., 2021). However, when acquiring and processing high-resolution DSMs over large areas, limitations due to drone endurance and computer processing capability increase the difficulty of operation and processing as the resolution required for flood simulation increases. This poses a significant practical challenge for researchers and professionals outside the surveying field (Abily et al., 2016). Therefore, considering simulation accuracy and efficiency, obtaining the optimal resolution that matches simulation requirements is more important than simply pursuing the highest resolution (Xing et al., 2018).

Since the gradual application of remote sensing images to hydraulic models, research on the effect of digital terrain data resolution on flood simulation has been a hot topic in this field. Saksena and Merwade (2015) used resampling technique and hydraulic model to analyse the relationship between a series of DEM resolutions from 3m to 100m and the extent of flood inundation in different rivers. They found that both the water surface elevation and the area of flood inundation show a positive linear relationship with DEM resolution. The coarser the resolution, the larger the inundation extent, leading to over-prediction. However, the application of this conclusion is limited to specific rivers and watershed characteristics, and some researchers found that when it comes to surface flooding (such as roads and towns along rivers), the relationship between DEM resolution and flood characteristic simulation results (such as range and depth) is not simply a positive linear one. At the same time, some studies have found that even if the resolution is the same, the simulation results of terrain data from different sources also show significant differences. Saksena and Merwade (2015) found that the simulation results of 30m DEM resampled from LiDAR DEM are much better than those directly using the publicly available 30m DEM from remote sensing images. These studies all indicate that discussing the effect of terrain data resolution on flood simulation requires restrictions on the target area and data source to improve the applicability of the conclusions (Shen and Tan, 2020).

Most previous studies have primarily focused on comparing errors in flood simulation characteristics (inundation area, depth), with a lack of discussion on the fundamental causes of simulation errors caused by different resolution data. For fluvial flood

https://doi.org/10.5194/egusphere-2024-404
Preprint. Discussion started: 22 March 2024

modelling in mountainous cities, the main factors affecting water flow should be the variation of river floodplains, riverside roads, and city streets and buildings with the undulation of the mountains. Considering the cost and difficulty of obtaining high-resolution terrain data, more in-depth discussions are generally centred around developed plains or coastal cities (Henonin et al., 2015; Xing et al., 2018; Leitao and De Sousa, 2018). The conclusions of these studies are basically around the impact of drainage network density, building size and gaps in different resolution DEMs on flood simulation, which is difficult to generalise to mountainous riverside cities affected by terrain undulation and rapid river level changes.

The objectives of this study are to: (a) discuss the application of high-resolution DSMs obtained by drones for fluvial flood modelling in the mountainous city; (b) use resampling techniques to examine the effect of DSMs obtained by drones at different resolutions on fluvial flood inundation simulation in the mountainous city; (c) analyse the representation of terrain features by DSMs at different resolutions based on topographic attributes, and investigate the fundamental causes of the effect. Ultimately, this study aims to provide support for the appropriate DSM resolution needed for fluvial flood modelling in mountainous cities.

2 Materials and methods

2.1 study area

The study area, Xuanhan, is a mountainous city located in the southwestern region of China, at the southern foot of the Daba Mountain. The built-up area of its main city is 23 km^2, with a population of 153,000 people. The city is located at the head of Zhou River, a primary tributary of the Qujiang River Basin, where the Qian River, Zhong River, and Hou River converge. At the confluence, there is a large reservoir which was fully completed and put into operation in 1992, with a regulation capacity of 102 million m^3 (Fig. 1). The county has an average annual rainfall of 1248 mm, with the rainy season accounting for over 80% of the total annual rainfall due to the influence of the rainstorm area of the Daba Mountain. The heavy rain mainly occurs from July to September. Between 1949 and 2021, the city experienced 14 major floods (peak flow of 6000-10000 m^3/s), with 1982, 2004, 2005 and 2010 being particularly severe floods (peak flow exceeding 10000 m^3/s). In the past decade, the floods caused by rainfall in the upstream Qian River, Zhong River, Hou River, and the discharge from the Jiangkou Reservoir have resulted in direct economic losses of more than 2 billion RMB (around 279 million US dollars).

As can be seen from the satellite map in Fig. 1, the study area is surrounded by water on three sides, and the city is distributed along the slopes, making it a typical mountainous riverside city. According to the 2022 Flood Control Plan of Xuanhan

https://doi.org/10.5194/egusphere-2024-404
Preprint. Discussion started: 22 March 2024

(Xuanhan County People's Government, 2022), this study delineates a drone survey and flood inundation simulation area that extends along the river to the left and right banks. This area covers six warning points corresponding to the discharge flow of the Jiangkou Reservoir and the inundation points of the city, as shown in Fig. 1 and Table 1. This series of inundation points is distributed in the upper, middle, and lower positions of the simulation area and can be used for subsequent inundation simulation verification. The selected flood event is a typical flood process obtained by the local hydrological bureau based on the analysis of the severe flood events in 2005 and 2010, and the rising process of the flood event includes the flow values corresponding to six inundation points.

2.2 drone images acquisition and processing for generating DSM

The general process of drone image acquisition and processing is shown in Fig. 2, and the drone flight campaign was flown on January 10, 2023, when the study area was in the winter dry season, with shallow river depths and large areas of exposed riverbeds. The DJI Matrice 300 RTK equipped with a Ruibo five-lens oblique photography sensor was used for the drone survey. The DJI Pilot 2 was used as the flight control program to set automatic flight paths and shooting parameters. In order to minimize the influence of building obstructions in the survey area, the flight altitude was set to 200 m, and the overlaps for the images were set at 80% for the longitudinal direction and 70% for the side direction (Cunliffe et al., 2016). Finally, 1467 vertical images were obtained, and the ground sample distance was 3 cm.

The ground control points (GCPs) were plotted using the Hi-Target GNSS receiver in real-time kinematic (RTK) positioning mode. DJI Terra was used to process the drone images, using five control points to optimize the sensors' position and direction data, and further check the positional accuracy. The final output products were orthoimages and initial DSM. PCI Geomatica was used to filter out noise on vegetation, water surfaces, and roads in the initial DSM. Considering the need for flood inundation simulation, all buildings along the riverbank were retained. To maximize the preservation of spatial details, all processing steps are carried out using the highest quality settings. However, there was still a certain degree of accuracy loss, and the final spatial resolution of the DSM was 6 cm, it was then resampled to produce coarser DSMs with 1 m, 5 m, 10 m, 15 m and 30 m resolutions.

Currently, sensors mounted on drones are unable to penetrate the water surface for underwater terrain surveys, and the underwater terrain still needs to be combined with bathymetric surveys and terrain interpolation. In this study, an unmanned boat equipped with a single beam sonar system was used to measure the underwater cross-section of the non-dried river section. Based on the research of Zhao et al. (2017), during the dry season, drones could be used to capture the downward trend of the

https://doi.org/10.5194/egusphere-2024-404
Preprint. Discussion started: 22 March 2024

exposed river floodplains on both sides of the river cross-section. Combined with the measured water depth, the underwater cross-section of the river is generalised into rectangular, trapezoidal, or arc shapes (Fig. 3). The complete underwater terrain data was obtained through cross-section interpolation, and the interpolation correction can be implemented through the terrain processing tool RAS Mapper.

2.3 Flood inundation modelling

The hydraulic model used in this study is the Hydrologic Engineering Center's River Analysis System (HEC-RAS) model, version 6.3.1. HEC-RAS is developed by the Hydrologic Engineering Center of the U.S. Army Corps of Engineers (U.S. Army Corps of Engineering, 2016). This software allows you to perform one-dimensional steady flow, one- and two-dimensional unsteady flow hydraulics modelling, sediment transport/mobile bed computations, water temperature modelling, and generalised water quality modelling (U.S. Army Corps of Engineering, 2016). It is one of the most widely used hydraulic models globally that is publicly available. This model includes two computational solvers, the two-dimensional Saint-Venant equations (Equation 1) and the two-dimensional diffusion wave equation (Equation 2). The vector forms of the momentum equations are as follows:

$$\frac{\partial \boldsymbol{V}}{\partial t} + (\boldsymbol{V} \cdot \nabla)\boldsymbol{V} + f_c \boldsymbol{k} \times \boldsymbol{V} = -g\nabla z_s + \frac{1}{h}\nabla \cdot (\boldsymbol{v}_t h \nabla \boldsymbol{V}) - \frac{\tau_b}{\rho R} + \frac{\tau_s}{\rho h} - \frac{1}{\rho}\nabla p_a \tag{1}$$

$$\frac{g n^2}{R^{4/3}} |\mathbf{V}|\mathbf{V} = -g\nabla Z_s - \frac{1}{\rho}\nabla p_a + \frac{\tau_s}{\rho h} \tag{2}$$

where here the velocity vector is $\boldsymbol{V} = (u, v)^T$, $\boldsymbol{v}_t$ is the eddy viscosity tensor, ∇ is the gradient operator, $\boldsymbol{k}$ is the unit vector in the vertical direction, $\boldsymbol{\tau}_b$ and $\boldsymbol{\tau}_s$ is the bottom shear and wind surface stress vector, h is water depth, f_c is coriolis parameter, p_a is atmospheric pressure, R is hydraulic radius, Z_s is water surface elevation, g is gravitational acceleration, n is manning's roughness coefficient, ρ is water density.

The 2D unsteady flow equation solvers both use the implicit finite volume solution algorithm. The implicit solution algorithm allows for a larger computational time step than explicit methods. Compared with traditional finite difference and finite element techniques, the finite volume method significantly improves the stability and robustness of the solution process (Mourato et al., 2021). For specific model introductions and usage, please refer to the HEC-RAS Applications Guide and HEC-RAS User's Manual (U.S. Army Corps of Engineering, 2016).

The flood inundation modelling in this study used a full two-dimensional unsteady flow model. Figure 4 shows the topographic data of the area, the two-dimensional computational grid, and the upstream and downstream boundary

https://doi.org/10.5194/egusphere-2024-404
Preprint. Discussion started: 22 March 2024

conditions (blue line in Fig. 4). The input data for the upstream boundary of the model is a typical flood process with a time step of 1 hour. The normal water depth calculated using the river slope drop is used under the downstream boundary conditions. The downstream river slope drop is calculated based on the DSM obtained by the drone, which is 0.00084 m/m.

2.4 Topographic attributes analysis

Obtaining topographic attributes from digital terrain data is a common method for capturing digital terrain features, evaluating the quality of terrain data, and analysing the uncertainty of terrain representation in different resolution terrain data. There are more than ten commonly used topographic attributes, which are used in hydrological analysis, land use, and soil vegetation analysis. Each indicator uses different methods to describe the terrain structure and shape, and the undulation of the terrain directly affects the flow of water on the surface. Therefore, this study selected six topographic attributes closely related to hydraulic simulation and hydrological analysis, and further analysed the effect of DSMs of different resolutions on flood inundation simulation based on topographic attributes. The topographic attributes are: Elevation, Topographic Position Index (TPI), Terrain Ruggedness Index (TRI), Wind Exposition Index (WEI), Morphometric Protection Index (MPI), Vector Ruggedness Measure (VRM). The specific meanings are shown in Table 2.

Salekin et al. (2023) found that when extracting topographic attributes, it is much more reasonable to use the average value of the plot than to directly measure the centre point of the plot, as the latter has poor spatial representativeness. Therefore, this study established 894 square plots of 30 m x 30 m in the analysis area based on the coarsest resolution (30m) as the plot side length. This ensures that at the coarsest resolution, the calculation of the plot contains complete grid pixels, and at a finer resolution, each plot can contain multiple complete grid pixels. All geospatial processing and data extraction were performed using ArcGIS and the System for Automated Geoscientific Analysis (SAGA v8.5.1) (Conrad et al., 2015). The Mean Absolute Error (MAE) was used to analyse the differences in DSM topographic attributes at different resolutions:

$$\mathrm{MAE} = \frac{1}{m}\sum_{i=1}^{m}|x_i - y| \quad (3)$$

Where m is the total number of plots calculated, x_i is the average value of the topographic indicators of each plot in the resampled DSM, and y is the topographic attribute value as a benchmark and control value, i.e., the value of topographic attributes of the 6cm DMS obtained by the drone.

3 Results and discussion

https://doi.org/10.5194/egusphere-2024-404
Preprint. Discussion started: 22 March 2024

3.1 Performance of drone DSM in mountainous urban fluvial flood modelling

This study used the original high-precision DSM (6 cm) obtained by drone as the benchmark topographic data input into the HEC-RAS model for 2D flood inundation simulation. Through the investigation of historical flooding traces, inundation boundaries, and flooding depths on site, the historical flooding characteristics of six inundation points were obtained. These characteristics were used to verify the simulation results and adjust the model parameters. The elevation positions of the six inundation points increase with the corresponding flood flow, and their distribution covers the upper, middle, and lower parts of the study area, allowing the model results to be verified from different situations and different locations (Fig. 5).

The red line in Fig. 5 of the on-site photos is the historical flood inundation boundary line of the inundation point, which is obtained based on historical flood photos, inundation trace investigations, and local flood control plan. As shown in the flood mapping results in Fig. 5, flood inundation modelling and historical flood inundation boundary lines at the six inundation points fit well, indicating good consistency between the model simulation and actual flood inundation. Therefore, in subsequent analyses, the calibrated simulation results of the 6 cm DSM are used as the benchmark conditions for comparative analysis (flood inundation boundary line, inundation area, inundation depth).

3.2 Effects of different resolutions on flood modelling

3.2.1 Overall comparison of flood area and depth

The resampled DSMs (1 m, 5 m, 10 m, 15 m, and 30 m) were sequentially input into the HEC-RAS for flood inundation modelling. Figure 6 shows the flood inundation situation simulated by different resolution DSMs at the maximum flood peak flow (12700m^3/s). As shown in Fig. 6, it can be preliminarily seen that as the DSM resolution decreases from high to low, the inundation area and depth gradually show differences, and different changes in magnitude are presented within and outside the main river channel (floodplain and riverbank).

Figure 7 shows the trend in inundation area and mean flood depth at maximum flood peak flow (12700m^3/s) based on DSMs at different resolutions. As shown in Fig. 7(a), within the range of the main river channel, there is no obvious trend in the inundation area with the decrease of the DSM resolution, and only a slight fluctuation occurs. While the mean flood depth shows an obvious fluctuation when the resolution is greater than 5 m. The reason for the lack of significant trends in modelling results within the main channel should be: the coarsest resolution (30 m) used in the discussion is much smaller than the average river width (about 182 m) in the study area . Meanwhile, except for the exposed riverbed topographic data obtained

https://doi.org/10.5194/egusphere-2024-404
Preprint. Discussion started: 22 March 2024

by drone during the dry season, the rest of the underwater topography of the river channel was obtained by generalised cross-section interpolation based on the trend of the floodplain (obtained by the drone) combined with the maximum underwater depth (obtained by the unmanned boat), which has a limited capture of the undulating features of the underwater topography, resulting in insensitivity to the change in DSM resolution in the simulation of inundation in the main river channel. Although there is no clear change pattern, the fluctuation of the results also indicates that the impact of different DSM resolutions on flood inundation simulation is not a simple linear relationship.

As shown in Fig. 7(b), in the floodplain and riverbank outside the main channel, the inundation area shows a significant decreasing trend with the decrease of the DSM resolution. Taking the flood modelling result drawn at 6 cm DSM as a benchmark, the inundation area decreases by 0.65%, 1.62%, 3.38%, 4.25%, and 7.67% respectively from 1 m to 30 m DSMs. While the mean flood depth shows no obvious change at 1m and 5m DSMs, a clear increasing trend can be seen after the resolution is greater than 5 m, increasing by 2.21%, 4.31%, and 10.41% respectively from 10 m to 30 m. Overall, both the inundation area and mean flood depth show an obvious step change, namely, compared with the benchmark, the change magnitude at 1 m and 5 m DSMs is small and similar, the change magnitude at 10 m and 15 m DSMs is large and similar, and the change magnitude at 30 m DSM is the largest.

For the floodplains and riverbank in the mountain city, as the DSM resolution decreases, the simulated inundation area becomes smaller and the mean flood depth becomes greater. It indicates that the change in resolution significantly affects the characterisation of DSM topography. More notably, both the flood area and depth showed some stage changes in the whole mountainous urban fluvial flood modelling as shown in Fig. 7(a) and (b), and this was also supported by visualising inundation area at different DSM resolutions (Fig. 6). The possible reason for this phenomenon is that as the resolution becomes coarser, the topographic undulation of the inundation area changes from the original smooth trend to a step-like trend, thereby changing the process of flood inundation in the model. This step-like trend of topographic undulation also makes the relationship between resolution change and flood inundation characteristics present a non-linear relationship (step change). When the resolution changes from fine to coarse to a certain extent, this step-like change in topographic undulation can show a significant change.

3.2.2 Specific effects of different resolution the inundation points

To further analyse the effect of DSM resolution on mountainous urban fluvial flood modelling, we discussed the simulation results of six inundation points at different resolutions. Figure 8 shows the inundation modelling results at point C(11200m^3/s)

https://doi.org/10.5194/egusphere-2024-404
Preprint. Discussion started: 22 March 2024

produced using different resolution DSMs, we identify the inundation situation simulated at this point with a 6 cm DSM as the benchmark and reference, and the red line in Fig. 8 represents the inundation boundary line at this point of the benchmark, i.e. the standard/control inundation boundary line.. By comparing the modelling results of different resolutions at point C, it was found that the simulation performance of using 1 m and 5 m DSMs at this point presents a better fit to the benchmark boundary line than that of other resolutions, and the corresponding inundation boundaries almost coincide with the benchmark. However, the simulation performance of using 15m and 30m DSMs at this point is substandard, and the corresponding inundation boundaries are far from the benchmark. The inundation boundary simulated using the 10 m DSM slightly exceeds the boundary line of the benchmark. Although it basically coincides at 10 m DSM, the flood depth at this point is greater than the benchmark (the colour is deeper than the benchmark).

Table 3 presents the comparison of simulation results at six inundation points using DSMs of different resolutions with the benchmark. A horizontal comparison of the results in Table 3 reveals that the larger the simulated discharge (the higher the elevation of the inundation point), the greater the impact of DSM resolution changes on the accuracy of the inundation simulation. When simulating the minimum discharge of 6000m^3/s (point F), all simulated inundation boundaries are in coincidence with the benchmark boundary (colors are green) using DSMs from 1 m to 15 m. However, when simulating the maximum discharge of 12700m^3/s (point A), only the simulation result corresponding to the 1 m DSM is coincident. For points where the simulated inundation boundary is not in coincidence with the benchmark, the average distance of the simulated boundary from the reference boundary basically tends to increase as the resolution becomes coarser.

A vertical comparison of simulation results at different resolutions in Table 3 reveals that the inundation boundary simulated using a 1 m DSM is in perfect coincidence with the benchmark with minimal error in the flood depth. The inundation boundaries produced using 5 m and 10 m DSMs are basically consistent with the benchmark at all inundation points except at some extreme discharges, but the flood depth simulated using a 10 m DSM is much greater than the depth at a finer resolution. It is clear that DSMs of 15 m and 30 m cannot meet the requirements for mountainous urban fluvial flood modelling.

Considering the results of Fig. 7 and Table 3, it can be seen that the simulation effect of flood characteristics shows a certain step change with the change of DSM resolution in the mountainous urban fluvial flood modelling. When the resolution is greater than 10 m, the simulation results of its flood characteristics cannot meet the requirements of flood inundation modelling in the mountainous riverside city. When the resolution does not exceed 5 m, its simulation results basically meet the requirements, and the results obtained by simulating with a 1 m DSM are in general coincidence with the results of centimetre-

https://doi.org/10.5194/egusphere-2024-404
Preprint. Discussion started: 22 March 2024

level DSM simulation. However, the simulation results using a 10 m DSM are basically qualified in terms of inundation boundaries, but there is an overestimation of the flood depth compared to 1 m and 5 m DSM.

3.3 Analysing the causes of effects based on topographic attributes

Floods in mountainous riverside cities are mainly caused by rapid confluence of flash floods driven by heavy rain. To further analyse the fundamental reasons for the impact of different resolution DSMs on the simulation of flood inundation in mountainous riverside cities, six topographic attribute indicators, namely, elevation, TPI, TRI, WEI, MPI, and VRM were selected to statistically analyse the topographic attributes of DSMs at different resolutions. Table 4 presents the statistical results of the topographic features of the 6 cm DSM, reflecting the topographic undulation of the study area from multiple perspectives. For example, TPI represents the difference in height between the grid and the average height of the surrounding grids, with a range from -2.87 to 28.51, and the average value is close to 0, indicating that the topography of this area is significantly undulating, with certain distributions of high and low lands. The filtered DSM retains buildings for flood modelling, so variables such as WEI, MPI, or VRM that describe steep ridge sites as well as accumulation areas can also be used to characterise the DSM's capture of mountainous buildings and bare ground.

Based on the topographic attributes of the 6 cm DSM as the benchmark, the characterisation of the topographic attributes of the study area by the 1m to 30 m DSM was analysed. Figure 9 shows the distribution of absolute errors for the six topographic attribute metrics calculated based on 1m to 30 m DSM in 894 square plots, and Table 5 presents the final MAE values. The results show that as the resolution of the DSM becomes coarser, the overall error between the six topographic attribute indicators and the benchmark increases. As shown in Fig. 9(a), (d), (e), and (f), the four indicators (elevation, WEI, MPI, and VRM) show a significant step change around a resolution of 10 m, and the errors corresponding to 5 m and 10 m are not much different. However, in the results of the remaining two indicators, TPI and TRI, the error corresponding to 10 m is much greater than the error corresponding to 5 m. This suggests that there is a certain threshold for the effect of DSM resolution changes on topographic attributes. Compared to DSMs with a resolution exceeding 10 m, DSMs with a resolution within 10 m can better capture the undulating features of the topography in the study area, which is crucial for the modelling of the inundation area. However, if features with specific elevation difference values are involved (such as TPI and TRI), it is best to keep the resolution within 5 m, which will have a direct impact on the accuracy of the modelling of the flood depth.

Considering the previous flood inundation modelling situation, it was found that as the resolution changes, there is consistency

https://doi.org/10.5194/egusphere-2024-404
Preprint. Discussion started: 22 March 2024

between the simulation results of flood inundation characteristics and the changes in topographic attributes. This indicates that the effect of DSM resolution on inundation modelling is mainly related to the complexity and undulation of the terrain, and the simulation accuracy is directly related to whether the DSM can accurately capture topographic features. The analysis of topographic attributes provides theoretical support for obtaining the optimal resolution to match simulation requirements. For mountainous urban fluvial flood modelling, sing the DSM obtained by drones as the terrain input, the resolution within 10 m can basically meet the simulation needs of the inundation area, since the DSM within this resolution can accurately characterise the features of the undulating and complex terrain (including buildings). However, considering the simulation needs of the flood depth and balancing the computational cost and the simulation requirements, the resolution of 1 m to 5 m can present better results, since the DSM with this resolution can accurately capture the characteristics of the specific difference in the elevation.

4 Conclusion

This study conducted a 2D flood inundation simulation of a mountainous riverside city in southwest China based on high-precision DSM obtained by drone. Considering the local government's flood prevention plan, field investigation of historical inundation traces, and inundation boundaries, the flood inundation simulation area and six inundation points for model validation were determined. The results showed that the flood inundation simulation and the historical flood inundation boundary lines at the six inundation points were well matched, and there was a good consistency between the model simulation results and the actual flood inundation.

The initial 6 cm DSM obtained by drone was resampled into 1 m, 5 m, 10 m, 15 m and 30 m DSM, respectively, as the terrain input for the 2D flood inundation simulation, and the effect of different resolutions on mountainous urban fluvial flood modelling was discussed. The results showed that, in the floodplain and riverbank outside the main channel, the inundation area showed a significant decreasing trend with the decrease of resolution. The mean flood depth did not change significantly at 1 m and 5 m DSM, but showed a significant increasing trend after the resolution was greater than 5 m. Both inside and outside the river channel showed a certain step change.

Similarly, based on the 6 cm DSM as the benchmark, the characterisation of topographic attributes by different resolution DSMs was further analysed. We found that there was a certain threshold for the effect of DSM resolution on topographic attributes. Compared with the DSM with a resolution of more than 10 m, the DSM with a resolution of less than 10 m could better capture the undulating and complex terrain features of the study area, especially within 5 m.

According to the analysis of terrain attributes, using the DSM obtained by drone to conduct a mountainous urban fluvial flood modelling, the resolution of the terrain data used should be kept within 1 m to 5 m. However, if larger watersheds and larger mountainous cities were involved, in the case of non-extreme discharges, considering the cost of acquisition and processing, using a resolution of 5 m to 10 m could also meet certain requirements in terms of inundation area drawing, but there could be a possibility of overestimation of flood depth.

Data availability. The hydrological data used in this study were provided by Sichuan Dazhou Hydrological and Water Resources Survey Centre.

Author contribution. XZ, TA, and XH suggested the idea and formulated the overarching research goals and aims. XY and XH operated the drone to get the image data. XZ, LM, and HY processed, corrected and managed the data. XZ prepared the manuscript with contributions from all co-authors.

Competing interests. The contact author has declared that neither they nor their co-authors have any competing interests.

Disclaimer. The opinions expressed here are those of the authors and not those of other individuals or organizations.

Financial support. This research has been supported by Sichuan University-Dazhou Municipal People's Government Strategic cooperation special fund project (grant nos. 2021CDDZ-12).

Reference

Abily, M., Bertrand, N., Delestre, O., Gourbesville, P., and Duluc, C.-M.: Spatial Global Sensitivity Analysis of High Resolution classified topographic data use in 2D urban flood modelling, Environ. Modell. Softw., 77, 183-195, https://doi.org/10.1016/j.envsoft.2015.12.002, 2016.

Acharya, B. S., Bhandari, M., Bandini, F., Pizarro, A., Perks, M., Joshi, D. R., Wang, S., Dogwiler, T., Ray, R. L., Kharel, G., and Sharma, S.: Unmanned Aerial Vehicles in Hydrology and Water Management: Applications, Challenges, and Perspectives, Water Resour. Res., 57, https://doi.org/10.1029/2021WR029925, 2021.

Alderman, K., Turner, L. R., and Tong, S.: Floods and human health: A systematic review, Environ. Int., 47, 37-47,

https://doi.org/10.5194/egusphere-2024-404
Preprint. Discussion started: 22 March 2024

https://doi.org/10.1016/j.envint.2012.06.003, 2012.

Azizian, A. and Brocca, L.: Determining the best remotely sensed DEM for flood inundation mapping in data sparse regions, Int. J. Remote Sens., 41, 1884-1906, https://doi.org/10.1080/01431161.2019.1677968, 2020.

Bates, P. D.: Integrating remote sensing data with flood inundation models: how far have we got?, Hydrol. Processes, 26, 2515-2521, https://doi.org/10.1002/hyp.9374, 2012.

Castaldi, F., Pelosi, F., Pascucci, S., and Casa, R.: Assessing the potential of images from unmanned aerial vehicles (UAV) to support herbicide patch spraying in maize, Precis. Agric., 18, 76-94, https://doi.org/10.1007/s11119-016-9468-3, 2017.

Conrad, O., Bechtel, B., Bock, M., Dietrich, H., Fischer, E., Gerlitz, L., Wehberg, J., Wichmann, V., and Boehner, J.: System for Automated Geoscientific Analyses (SAGA) v. 2.1.4, Title Geosci. Model Dev., 8, 1991-2007, https://doi.org/10.5194/gmd-8-1991-2015, 2015.

Cook, A. and Merwade, V.: Effect of topographic data, geometric configuration and modelling approach on flood inundation mapping, J. Hydrol., 377, 131-142, https://doi.org/10.1016/j.jhydrol.2009.08.015, 2009.

Cook, K. L.: An evaluation of the effectiveness of low-cost UAVs and structure from motion for geomorphic change detection, Geomorphology, 278, 195-208, https://doi.org/10.1016/j.geomorph.2016.11.009, 2017.

Corringham, T. W. and Cayan, D. R.: The Effect of El Nino on Flood Damages in the Western United States, Weather Clim. Soc., 11, 489-504, https://doi.org/10.1175/WCAS-D-18-0071.1, 2019.

Cunliffe, A. M., Brazier, R. E., and Anderson, K.: Ultra-fine grain landscape-scale quantification of dryland vegetation structure with drone-acquired structure-from-motion photogrammetry, Remote Sens. Environ., 183, 129-143, https://doi.org/10.1016/j.rse.2016.05.019, 2016.

da Costa, R. T., Mazzoli, P., and Bagli, S.: Limitations Posed by Free DEMs in Watershed Studies: The Case of River Tanaro in Italy, Front. Earth Sci., 7, https://doi.org/10.3389/feart.2019.00141, 2019.

Güneralp, B., Güneralp, İ., and Liu, Y.: Changing global patterns of urban exposure to flood and drought hazards, Glob. Environ. Change-Human Policy Dimens., 31, 217-225, https://doi.org/10.1016/j.gloenvcha.2015.01.002, 2015.

Harris, A. and Baird, A. J.: Microtopographic Drivers of Vegetation Patterning in Blanket Peatlands Recovering from Erosion, Ecosystems, 22, 1035-1054, https://doi.org/10.1007/s10021-018-0321-6, 2019.

Henonin, J., Ma, H., Yang, Z.-Y., Hartnack, J., Havno, K., Gourbesville, P., and Mark, O.: Citywide multi-grid urban flood modelling: the July 2012 flood in Beijing, Urban Water J., 12, 52-66, https://doi.org/10.1080/1573062X.2013.851710, 2015.

Kumar, L., Skidmore, A. K., and Knowles, E.: Modelling topographic variation in solar radiation in a GIS environment, Int. J. Geogr. Inf. Sci., 11, 475-497, https://doi.org/10.1080/136588197242266, 1997.

Leitao, J. P. and de Sousa, L. M.: Towards the optimal fusion of high-resolution Digital Elevation Models for detailed urban flood assessment, J. Hydrol., 561, 651-661, https://doi.org/10.1016/j.jhydrol.2018.04.043, 2018.

Loladze, A., Augusto Rodrigues, F., Jr., Toledo, F., San Vicente, F., Gerard, B., and Boddupalli, M. P.: Application of Remote Sensing for Phenotyping Tar Spot Complex Resistance in Maize, Front. Plant Sci., 10, https://doi.org/10.3389/fpls.2019.00552, 2019.

Md Ali, A., Solomatine, D. P., and Di Baldassarre, G.: Assessing the impact of different sources of topographic data on 1-D hydraulic modelling of floods, Hydrol. Earth Syst. Sci., 19, 631-643, https://doi.org/10.5194/hess-19-631-2015, 2015.

Meesuk, V., Vojinovic, Z., Mynett, A. E., and Abdullah, A. F.: Urban flood modelling combining top-view LiDAR data with ground-view SfM observations, Adv. Water Resour., 75, 105-117, https://doi.org/10.1016/j.advwatres.2014.11.008, 2015.

Mourato, S., Fernandez, P., Marques, F., Rocha, A., and Pereira, L.: An interactive Web-GIS fluvial flood forecast and alert system in operation in Portugal, Int. J. Disaster Risk Reduct., 58, https://doi.org/10.1016/j.ijdrr.2021.102201, 2021.

Muthusamy, M., Casado, M. R., Butler, D., and Leinster, P.: Understanding the effects of Digital Elevation Model resolution in urban fluvial flood modelling, J. Hydrol., 596, https://doi.org/10.1016/j.jhydrol.2021.126088, 2021.

Ogania, J. L., Puno, G. R., Alivio, M. B. T., and Taylaran, J. M. G.: Effect of digital elevation model's resolution in producing flood hazard maps, Glob. J. Environ. Sci. Manag., 5, 95-106, https://doi.org/10.22034/gjesm.2019.01.08, 2019.

Ozdemir, H., Sampson, C. C., de Almeida, G. A. M., and Bates, P. D.: Evaluating scale and roughness effects in urban flood modelling using terrestrial LIDAR data, Hydrol. Earth Syst. Sci., 17, 4015-4030, https://doi.org/10.5194/hess-17-4015-2013, 2013.

People's Government of Xuanhan County: Xuanhan County 2022 Flood Protection Plan, available at http://www.xuanhan.gov.cn/xxgk-show-64349.html (last accesse: January 2024), 2022.

Saksena, S. and Merwade, V.: Incorporating the effect of DEM resolution and accuracy for improved flood inundation mapping, J. Hydrol., 530, 180-194, https://doi.org/10.1016/j.jhydrol.2015.09.069, 2015.

Salekin, S., Bloomberg, M., Morgenroth, J., Meason, D. F., and Mason, E. G.: Within-site drivers for soil nutrient variability in plantation forests: A case study from dry sub-humid New Zealand, Catena, 200, https://doi.org/10.1016/j.catena.2021.105149, 2021.

Salekin, S., Lad, P., Morgenroth, J., Dickinson, Y., and Meason, D. F.: Uncertainty in primary and secondary topographic attributes caused by digital elevation model spatial resolution, Catena, 231, https://doi.org/10.1016/j.catena.2023.107320, 2023.

Salekin, S., Mason, E. G., Morgenroth, J., Bloomberg, M., and Meason, D. E.: Modelling the Effect of Microsite Influences on the Growth and Survival of Juvenile Eucalyptus globoidea (Blakely) and Eucalyptus bosistoana (F. Muell) in New Zealand, Forests, https://doi.org/10, 10.3390/f10100857, 2019.

Samela, C., Manfreda, S., Paola Francesco, D., Giugni, M., Sole, A., and Fiorentino, M.: DEM-Based Approaches for the

Delineation of Flood-Prone Areas in an Ungauged Basin in Africa, J. Hydrol. Eng., 21, 06015010, https://doi.org/10.1061/(ASCE)HE.1943-5584.0001272, 2016.

Shen, J. and Tan, F.: Effects of DEM resolution and resampling technique on building treatment for urban inundation modelling: a case study for the 2016 flooding of the HUST campus in Wuhan, Nat. Hazards, 104, 927-957, https://doi.org/10.1007/s11069-020-04198-z, 2020.

Utlu, M. and Ozdemir, H.: How much spatial resolution do we need to model a local flood event? Benchmark testing based on UAV data from Biga River (Turkey), Arab. J. Geosci., 13, https://doi.org/10.1007/s12517-020-06318-2, 2020.

WHO: World Health Organisation - Flood [WWW Document], available at: https://www.who.int/health-topics/floods#tab=tab_1 (last accesse: December 2023), 2020.

Xing, Y., Liang, Q., Wang, G., Ming, X., and Xia, X.: City-scale hydrodynamic modelling of urban flash floods: the issues of scale and resolution, Nat. Hazards, 96, 473-496, https://doi.org/10.1007/s11069-018-3553-z, 2018.

Yan, K., Di Baldassarre, G., Solomatine, D. P., and Schumann, G. J. P.: A review of low-cost space-borne data for flood modelling: topography, flood extent and water level, Hydrol. Process., 29, 3368-3387, https://doi.org/10.1002/hyp.10449, 2015.

Zhao, C. S., Zhang, C. B., Yang, S. T., Liu, C. M., Xiang, H., Sun, Y., Yang, Z. Y., Zhang, Y., Yu, X. Y., Shao, N. F., and Yu, Q.: Calculating e-flow using UAV and ground monitoring, J. Hydrol., 552, 351-365, https://doi.org/10.1016/j.jhydrol.2017.06.047, 2017.

https://doi.org/10.5194/egusphere-2024-404
Preprint. Discussion started: 22 March 2024

Table 1 Flood inundation points in Xuanhan City

Serial number	Discharge flow of the Jiangkou Reservoir	Location of inundation point	Serial number	Discharge flow of the Jiangkou Reservoir	Location of inundation point
A	$12700m^3/s$	The gate of the Local Tax Bureau	D	$9800m^3/s$	The Wangjia square
B	$12000m^3/s$	The entrance of China Construction Bank	E	$7000m^3/s$	Riverwalk outside the Lower Town Street
C	$11200m^3/s$	The gate of Red Army Memorial Park	F	$6000m^3/s$	Riverwalk outside the Westside Police Station

https://doi.org/10.5194/egusphere-2024-404
Preprint. Discussion started: 22 March 2024

Table 2 Description of topographic variables used as independent explanatory variables for modelling. Descriptions are based on Salekin et al., (2021), Harris and Baird (2019), and the SAGA-GIS Tool Library Documentation (v8.5.1).

Topographic variables	Description	Formula/Units
Elevation	Elevation above sea level in meters.	Meters
Topographic Position Index	Difference between elevation of the cell and the mean of the elevation in surrounding cells, calculated by dividing the elevation difference by its standard deviation.	No unit Value > 0 when the cell is higher than its surroundings,zero when in a flat area or mid-slope and < 0 when lower than its surroundings.
Terrain ruggedness index	A measure of terrain complexity/ heterogeneity. It calculates the sum change in elevation between a grid cell and its neighbouring grid cells.	Meters Value is always ≥0 m, where 0 represents the minimum roughness
Wind Exposition Index	Calculates the average wind effect across all directions using an angular step.	No unit Value < 1 indicates wind-shadowed ar eas, value > 1 indicates areas expose d to wind.
Morphometric Protection Index	Analyses the immediate surrounding of each cell up to a given distance and evaluates how the relief protects it.	No unit Value > 0 when the cell is protected and < 0 when it is not.
Vector ruggedness measure	A measure of terrain complexity/vari ance that captures variability in slop e and aspect in a single measure.	No unit Natural terrain has values between 0 and 0.4

https://doi.org/10.5194/egusphere-2024-404
Preprint. Discussion started: 22 March 2024

Table 3 modelling results of inundation boundary line and flood depth produced using different resolution DSMs at six inundation points

Inundation point	Discharge (m^3/s)	Simulation results at different DSM resolution					
		0.06m	1m	5m	10m	15m	30m
A	12700	0	-0.09m	8.3m	9.8m	12.2m	16.8m
B	12000	0	0.06m	0.07m	4.5m	14.0m	14.0m
C	11200	0	0.05m	0.10m	0.71m	87m	34m
D	9800	0	0.03m	-0.02m	0.19m	5.1m	37.1m
E	7000	0	0.01m	0.02m	0.17m	11.5m	25.7m
F	6000	0	-0.03m	0.03m	0.50m	1.10m	8.0m

Note: The green colour indicates that the simulated inundation boundary is in coincidence with the benchmark boundary , and the numbers inside indicate the average error between the simulated inundation boundary's flood depth and the benchmark; the red colour indicates that the simulated inundation boundary is not in coincidence, and the numbers inside indicate the average distance that the simulated inundation boundary differs from the benchmark.

https://doi.org/10.5194/egusphere-2024-404
Preprint. Discussion started: 22 March 2024

Table 4 Summary of the topographic attributes index for the standard（6cm DSM）

Topographic attribute index	6cm DSM			
	Min	Max	Mean	SD
Elevation	262.29	355.70	290.64	16.23
TPI	-2.87	28.51	0.04	1.05
TRI	0.00	38.28	0.13	1.45
WEI	1.26	0.79	1.01	0.10
MPI	0.00	1.52	0.31	0.31
VRM	0.00	0.70	0.03	0.09

https://doi.org/10.5194/egusphere-2024-404
Preprint. Discussion started: 22 March 2024

Table 5 MAE of six topographic attribute metrics at different resolutions

topographic attribute index	MAE results at different DSM resolution				
	1m	5m	10m	15m	30m
Elevation	0.404	1.403	**1.617**	5.438	8.255
TPI	1.024	**3.412**	5.485	6.957	9.734
TRI	1.437	**5.014**	8.024	10.140	14.102
WEI	0.034	0.075	**0.083**	0.105	0.121
MPI	0.148	0.253	**0.259**	0.321	0.312
VRM	0.070	0.100	**0.109**	0.143	0.115

Note: Bold black values indicate abrupt/step changes before and after the value.

https://doi.org/10.5194/egusphere-2024-404
Preprint. Discussion started: 22 March 2024

Fig.1

Location of study area, Xuanhan City, China, and the flood core control area (yellow boundary line) shown on the satellite map (from ©Google Earth) and the orthophoto, including drone survey area, flood modelling area and six inundation points

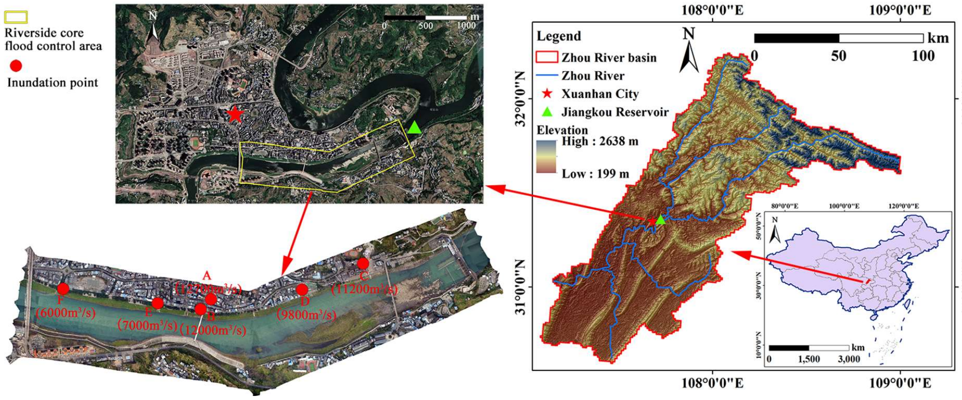

https://doi.org/10.5194/egusphere-2024-404
Preprint. Discussion started: 22 March 2024

Fig.2

Flowchart of drone images acquisition and processing

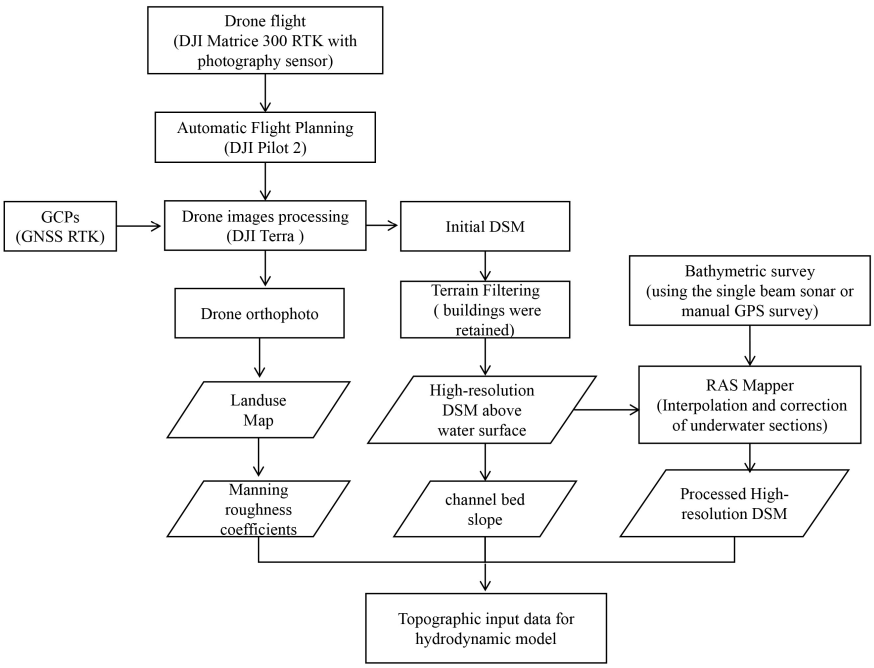

https://doi.org/10.5194/egusphere-2024-404
Preprint. Discussion started: 22 March 2024

Fig.3

Generalization of the underwater cross-section

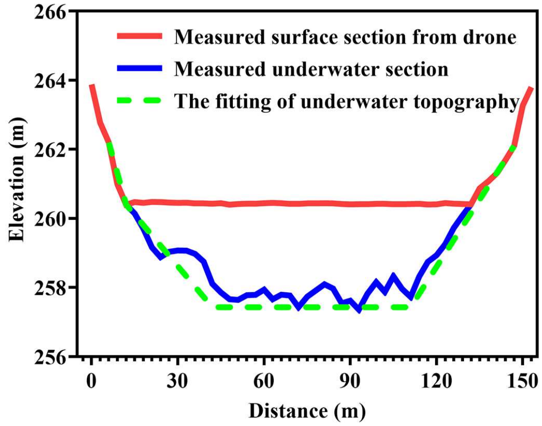

https://doi.org/10.5194/egusphere-2024-404
Preprint. Discussion started: 22 March 2024

Fig.4

Mesh used for all simulations with 6 cm DSM in the HEC-RAS and hydrograph of the typical flood event

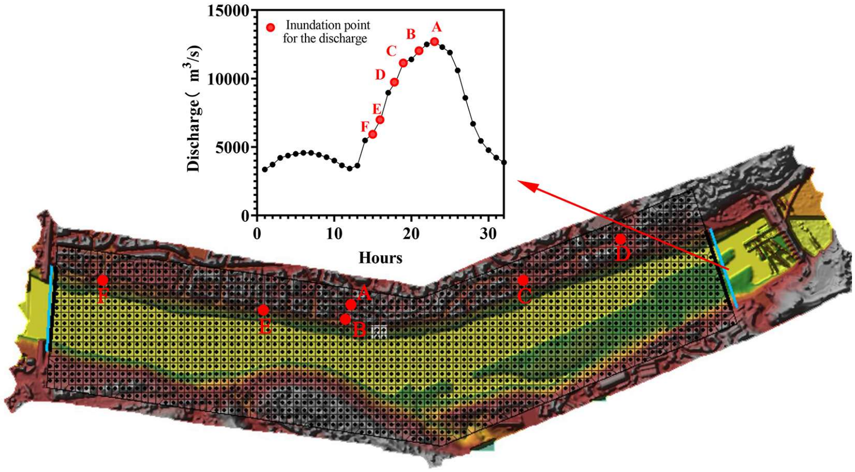

https://doi.org/10.5194/egusphere-2024-404
Preprint. Discussion started: 22 March 2024

Fig.5

Comparison and validation of inundation point simulation results with historical flood boundary lines (The inner six images are on-site survey images about six inundation points and the outer six localized magnified orthophotos are the corresponding flood mapping results from HEC-RAS)

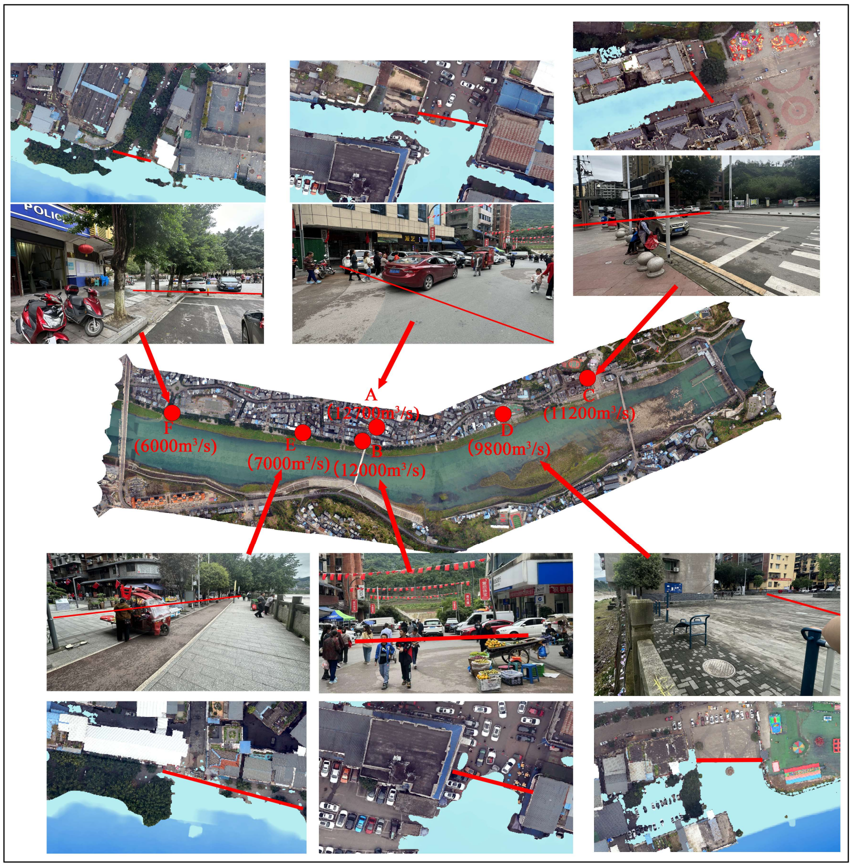

https://doi.org/10.5194/egusphere-2024-404
Preprint. Discussion started: 22 March 2024

Fig. 6

Flood inundation obtained by inputting different resolution DSM for hydraulic modelling (resolutions ranging from 6 cm to 30 m)

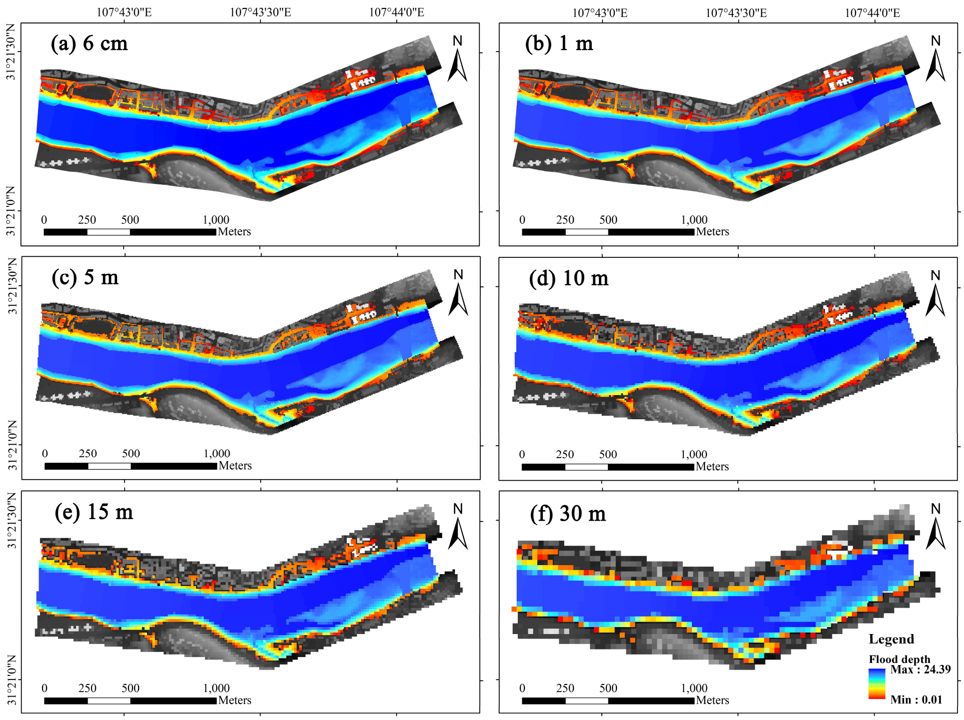

https://doi.org/10.5194/egusphere-2024-404
Preprint. Discussion started: 22 March 2024

Fig. 7

Trend of the inundation area and mean flood depth derived from DSMs with different resolution at the flood peak (a) main river channel, (b) floodplain and riverbank (out of main river channel)

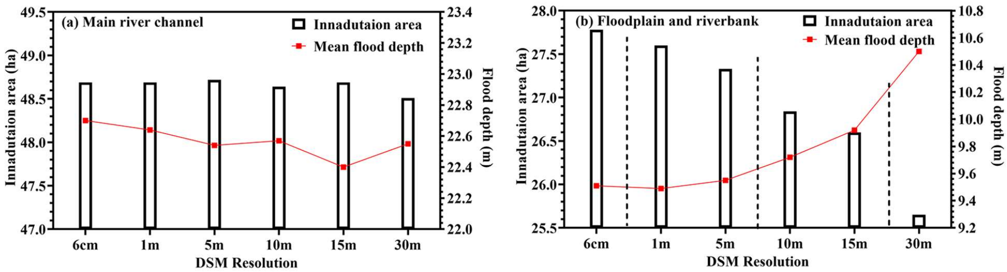

https://doi.org/10.5194/egusphere-2024-404
Preprint. Discussion started: 22 March 2024

Fig. 8

Inundation modelling results at point C(11200m^3/s) produced using different resolution DSMs

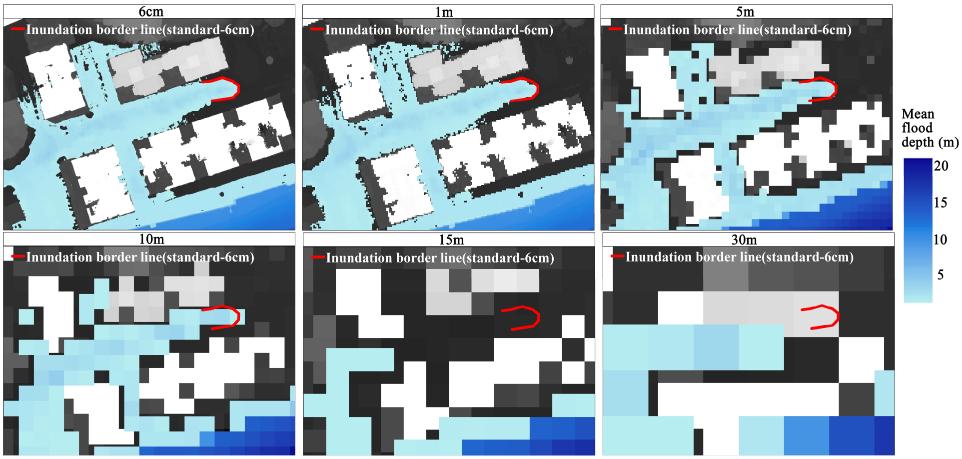

https://doi.org/10.5194/egusphere-2024-404
Preprint. Discussion started: 22 March 2024

Fig. 9

Variations in absolute errors for topographic features derived at different resolutions of DSMs

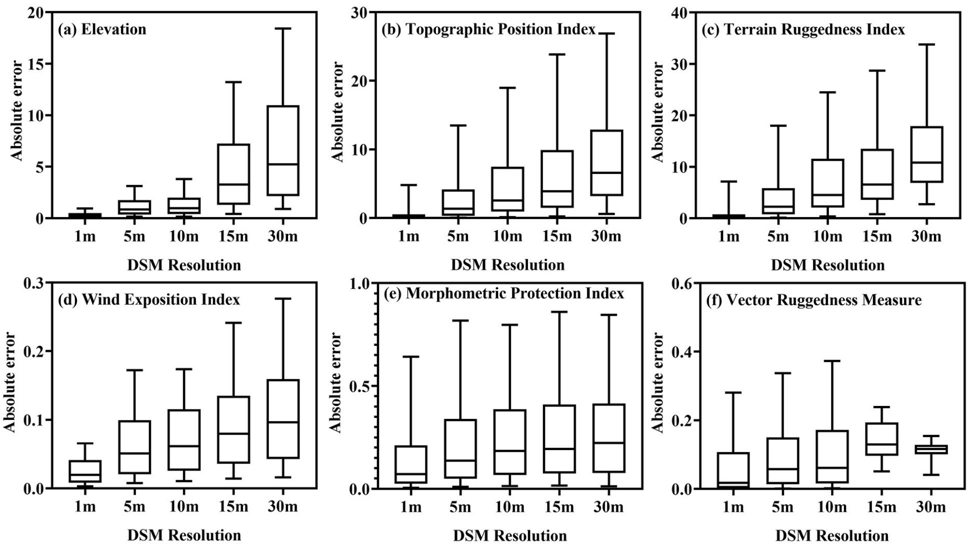

https://doi.org/10.5194/egusphere-2024-404
Preprint. Discussion started: 22 March 2024

figure captions

Fig.1 Location of study area, Xuanhan City, China, and the flood core control area (yellow boundary line) shown on the satellite map (from ©Google Earth) and the orthophoto, including drone survey area, flood modelling area and six inundation points

Fig. 2 Flowchart of drone images acquisition and processing

Fig.3 Generalization of the underwater cross-section

Fig.4 Mesh used for all simulations with 6 cm DSM in the HEC-RAS and hydrograph of the typical flood event

Fig. 5 Comparison and validation of inundation point simulation results with historical flood boundary lines (The inner six images are on-site survey images about six inundation points and the outer six localized magnified orthophotos are the corresponding flood mapping results from HEC-RAS)

Fig.6 Flood inundation obtained by inputting different resolution DSM for hydraulic modelling (resolutions ranging from 6 cm to 30 m)

Fig.7 Trend of the inundation area and mean flood depth derived from DSMs with different resolution at the flood peak (a) main river channel, (b) floodplain and riverbank (out of main river channel)

Fig. 8 Inundation modelling results at point C(11200m^3/s) produced using different resolution DSMs

Fig. 9 Variations in absolute errors for topographic features derived at different resolutions of DSMs